Supplementary Information

A Robust Heterometallic Ultramicroporous MOF with Ultrahigh Selectivity for Propyne/Propylene Separation

Yun-Lei Peng,[#a,b] Ting Wang,[#a] Chaonan Jin,[d] Pengfei Li,[a] Shanelle Suepaul,[e] Gary Beemer,[f] Yao Chen,[d] Rajamani Krishna,[g] Peng Cheng,[a,c] Tony Pham,[e,f] Brian Space,[e] Michael J. Zaworotko,[b] Zhenjie Zhang*[a,c,d]

Experimental Procedures

Materials and Methods

General Methods

Pyrazine (99%, innochem), $Cu(NO_3)_2{\cdot}3H_2O$ (Analytical reagent, Gerhardite), $(NH_4)_2{\cdot}SiF_6$ (Analytical reagent, Greagent), 4,4'-bipyridylacetylene (95+%, HUAWEIRUIKE), 4,4' -azopyridine (95+%, HUAWEIRUIKE), $CuSiF_6$ (Analytical reagent, Greagent), $Ni(BF_4)_2{\cdot}6H_2O$ (Energy chemical), 2,3-dichloropyrazine (98%, Bide Pharmatech Ltd), Sodium hydroxide (NaOH, 97%, Aladdin), Sodium hydrosulfide (NaHS, LiDeShi), Copper(II) perchlorate hexahydrate ($Cu(ClO_4)_2.6H_2O$, 98%, Strem Chemical, Inc.), Nickel(II) iodide (NiI_2, >99.5%, aladdin), iodide (I_2, AR, TIANJINGFENGCHUAN), acetonitrile, ether, and acetone were purchased and used without further purification. He, N_2, C_3H_4 and C_3H_6, were purchased from AIR LIQUIDE. The powder X-ray diffraction data were obtained on ULTIMA IV. Fourier transform infrared spectra (FT-IR) were recorded on Nicolet IS10.

Synthesis of metal-ligand $Na[Cu(pdt)_2]{\cdot}2H_2O$

The ligand was synthesized based on the previous method.[1]

Synthesis of SIFSIX-3-Ni $(Ni(pyrazine)_2SiF_6)_n$

SIFSIX-3-Ni were prepared based on previously reported procedures.[2a]

Synthesis of SIFSIX-2-Cu-i $(Cu(4,4'\text{-bipyridylacetylene})_2SiF_6)_n$

SIFSIX-2-Cu-i were prepared based on previously reported procedures.[2b]

Synthesis of SIFSIX-14-Cu-i (UTSA-200) $(Cu(4,4'\text{ -azopyridine})_2SiF_6)_n$

SIFSIX-14-Cu-i were prepared based on previously reported procedures. [2a]

Powder X-ray diffraction (PXRD) analysis:

Powder x-ray diffraction test was conducted using microcrystalline samples on a Rigaku Ultima IV diffractometer (40 kV, 40 mA, CuKα1, 2 λ = 1.5418 Å). The measured parameter included a scan speed of 2(°)/min, a step size of 0.02(°).

Field emission scanning electron microscope (FE-SEM) analysis:

The morphologies of **NKMOF-11** were characterized via field-emission scanning electron microscopy (SEM, JEOL JSM7500F, 5 kV and Phenom XL, 15 kV). The SEM–energy dispersive spectroscopy (EDS) of the samples are collected with Phenom XL at an acceleration voltage of 15 kV.

Inductively Coupled Plasma Optical Emission Spectro analysis

The metal element ratio in **NKMOF-11** was characterized by ICP-OES(SPECTRO-BLUE).

Fitting of single-component adsorption isotherm and Isosteric Heat of Adsorption

The experimental isosteric heat of adsorption (Q_{st}) values for various gases in **NKMOF-11** were determined by first fitting the adsorption isotherms at 273 K, 298 K, 308 K and 318 K for the respective adsorbates to the dual-site Langmuir-Freundlich (**DSLF**) equation,[3] subsequently applying the Clausius-Clapeyron method.[4] The **DSLF** equation is given by:

$$n = \frac{n_{m1} b_1 P^{\left(\frac{1}{t_1}\right)}}{1 + b_1 P^{\left(\frac{1}{t_1}\right)}} + \frac{n_{m2} b_2 P^{\left(\frac{1}{t_2}\right)}}{1 + b_2 P^{\left(\frac{1}{t_2}\right)}} \quad \text{(DSLF)} \qquad (1)$$

where n is the uptake (in mmol g^{-1}), P is the pressure (in kPa), n_{m1} and n_{m2} are the saturation uptakes (in mmol g^{-1}) for sites 1 and 2, b_1 and b_2 are the affinity coefficients (in kPa^{-1}) for sites 1 and 2, and t_1 and t_2 represent the deviations from the ideal homogeneous

surface (unit less) for sites 1 and 2. The parameters that were obtained from the fitting of the C_3H_4 and C_3H_6 adsorption isotherms are found in**Tables S1** and **S2,** respectively.
The fitted parameters were used to calculate the Q_{st} values for a range of uptakes through the Clausius–Clapeyron equation, which is the following:

$$Q_{st} = -R\frac{\partial \ln P}{\partial\left(1/T\right)} \quad (2)$$

Where T is the temperature (in K) and R is the ideal gas constant. The partial derivative term actually represents the slope of the plot of ln P *vs.* 1/T for a number of isotherms at different temperatures at various loadings. Therefore, the above Q_{st} equation can be simplified to:

$$Q_{st} = -mR \quad (3)$$

where m is the slope, which can be calculated by the following for x (2 or 3) different temperatures and their corresponding pressures:

$$m = \frac{\sum\frac{1}{T_i}\ln P_i - \frac{1}{x}\left(\sum\frac{1}{T_i}\right)\left(\sum \ln P_i\right)}{\sum\left(\frac{1}{T_i}\right)^2 - \frac{1}{x}\left(\sum\frac{1}{T_i}\right)^2} \quad (4)$$

The P_i values were back-calculated for a range of uptakes using the DSLF equation *via* an iterative technique (e.g., the Newton–Raphson method).[5]
The experimental C_3H_6 and C_3H_4 Q_{st} for **NKMOF-11** were also determined through a simultaneous fitting to the DSLF equation,[5] Notably, b_1 and b_2 are expressed as a function of temperature via the following:

$$b_1 = b_{01}e^{\left(\frac{E1}{RT}\right)} \quad (5)$$

$$b_2 = b_{02}e^{\left(\frac{E2}{RT}\right)} \quad (6)$$

where R is the ideal gas constant, b_{01} and E_1 are the pre-exponential factor (in kPa^{-1}) and the activation energy (in kJ mol^{-1}) for site 1, and b_{02} and E_2 are analogous parameters for site 2. The parameters obtained for the simultaneous fitting of the experimental C_3H_6 and C_3H_4 adsorption isotherms at 298 and 308 K in **NKMOF-11** are provided in **Tables S3 and S4**. These parameters were used to calculate the Q_{st} values for a range of uptakes using the following form of the Clausius-Clapeyron equation:

$$Q_{st} = \frac{-RT_1T_2}{T_2 - T_1}\ln\left(\frac{P_1}{P_2}\right) \quad (7)$$

Results and Discussion

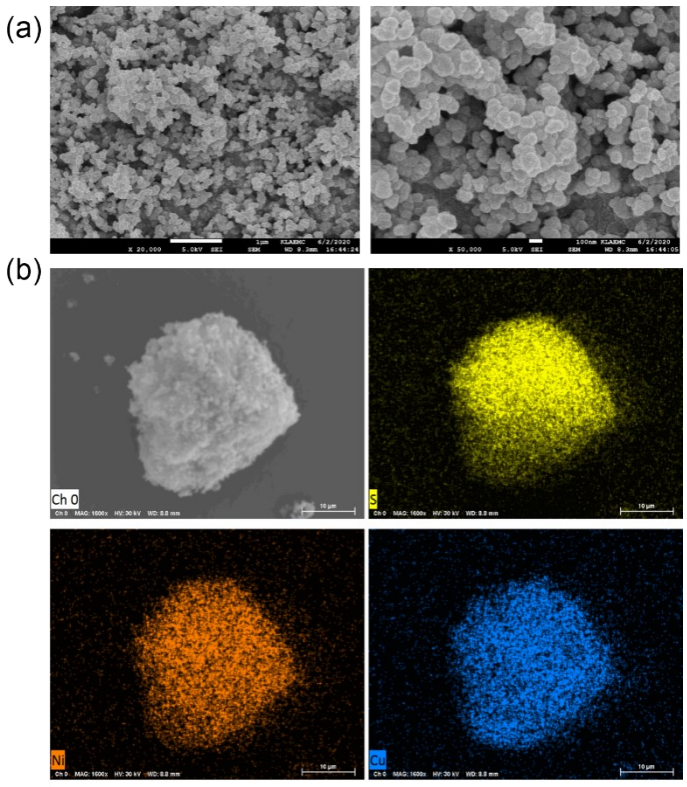

Fig. S1 (a) The field emission scanning electron microscope (FE-SEM) images of **NKMOF-11**; (b) The elemental mapping of **NKMOF-11**.

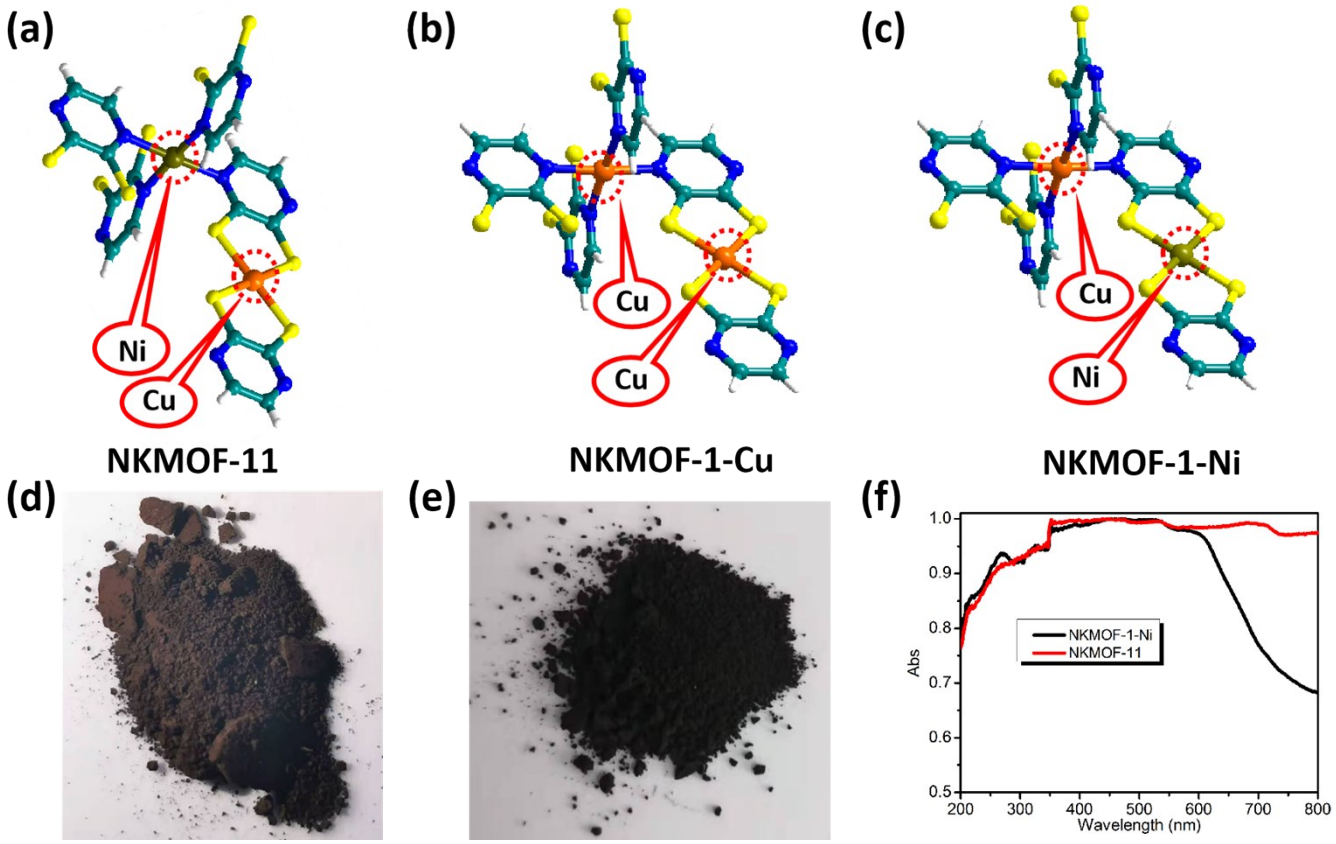

Fig. S2 (a) The coordination environment of metals in **NKMOF-11**.; (b) The coordination environment of metals in **NKMOF-1-Cu**; (c) The coordination environment of metals in **NKMOF-1-Ni; (d) The appearance of NKMOF-1-Ni; (e) The appearance of NKMOF-11; (F) The solid UV-Vis spectra of NMOF-11 and NKMOF-1-Ni.**

(a)

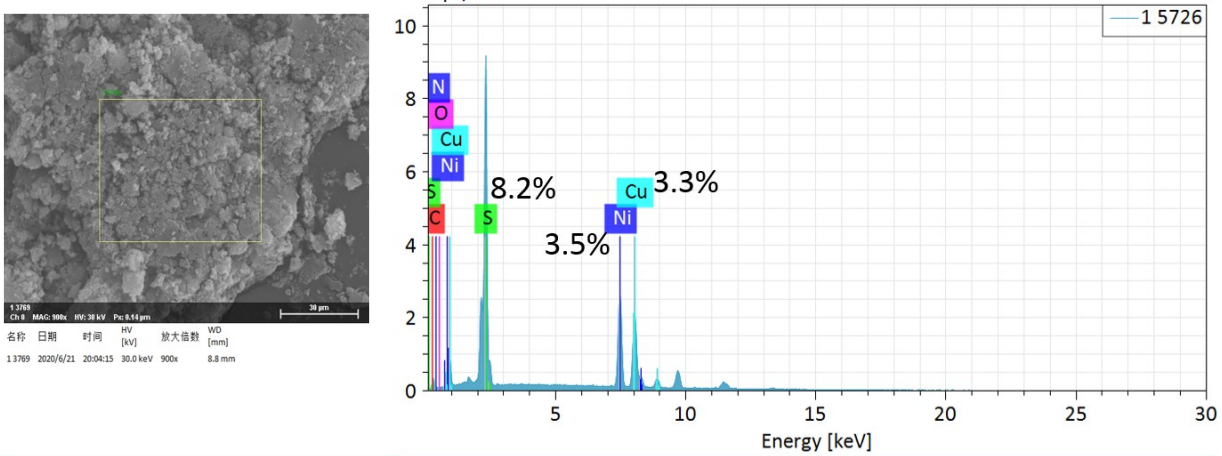

(b)

Instrument	ICP-OES（SPECTRO-BLUE）	
Testing Results (wt%)		
NKMOF-11	Cu	Ni
1	14.82	15.31
2	15.25	14.92
3	14.96	15.34
Average	15.01	15.19

Fig. S3 (a) Energy Dispersive X-ray Spectrometric Microanalysis (EDX) of **NKMOF-11**; (b) Inductively Coupled Plasma Optical Emission Spectro of **NKMOF-11**.

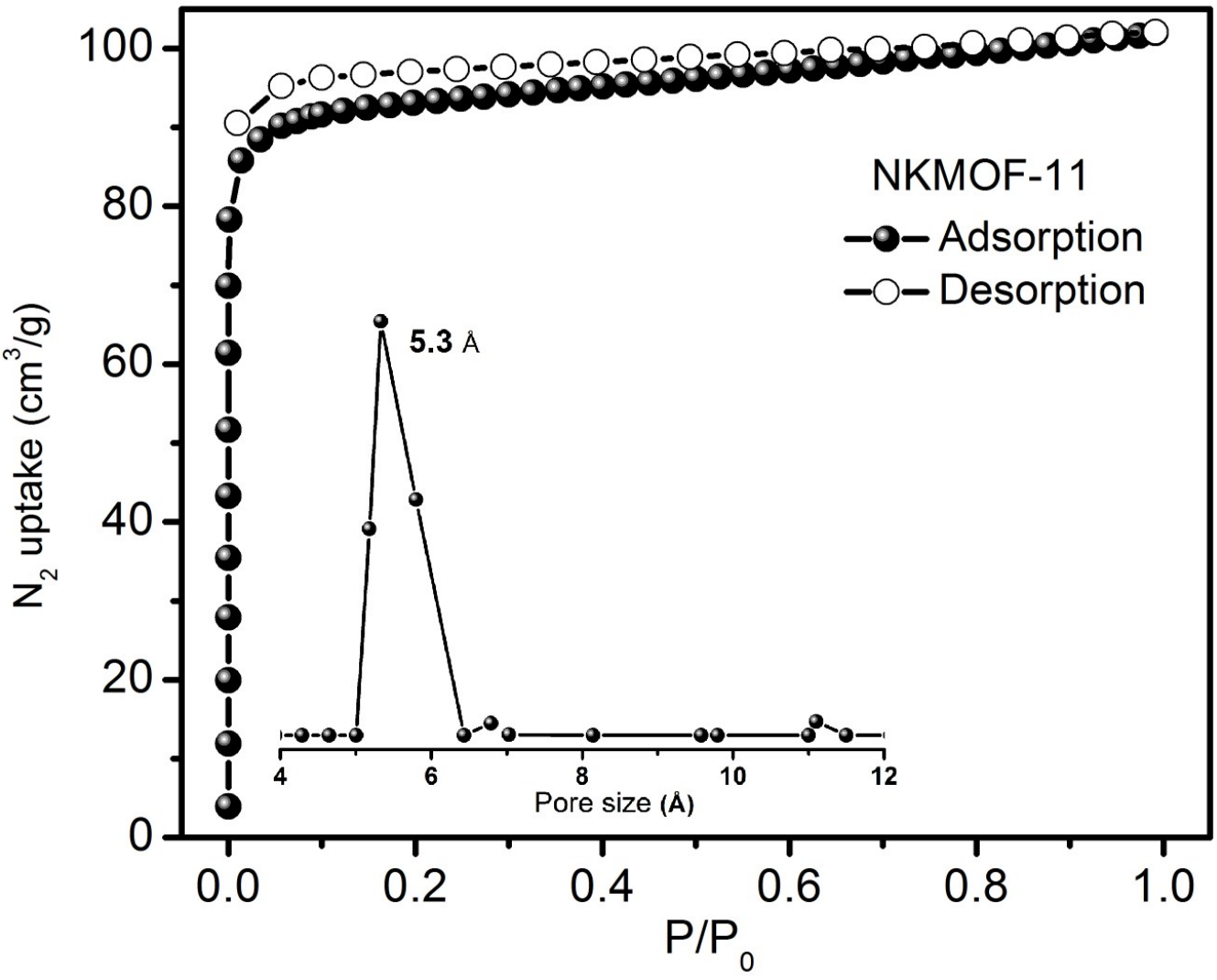

Fig. S4 N_2 adsorption isotherm and pore size distribution of **NKMOF-11** at 77 K.

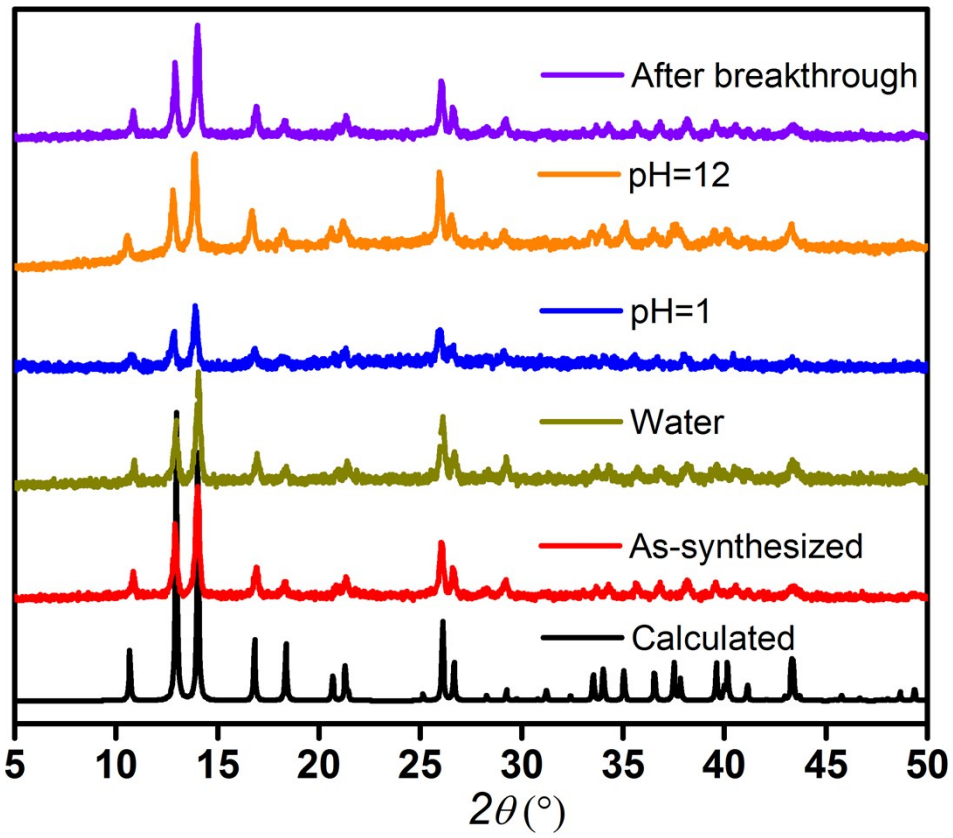

Fig. S5 PXRD patterns showing the exceptional structural stability of **NKMOF-11**. Pristine **NKMOF-11** (red); **NKMOF-11** soaked in pure water for 2 year (dark yellow); **NKMOF-11** soaked in pH=1 aqueous solution (blue); **NKMOF-11** soaked in pH=12 aqueous solution(orange); after fifth breakthrough (violet).

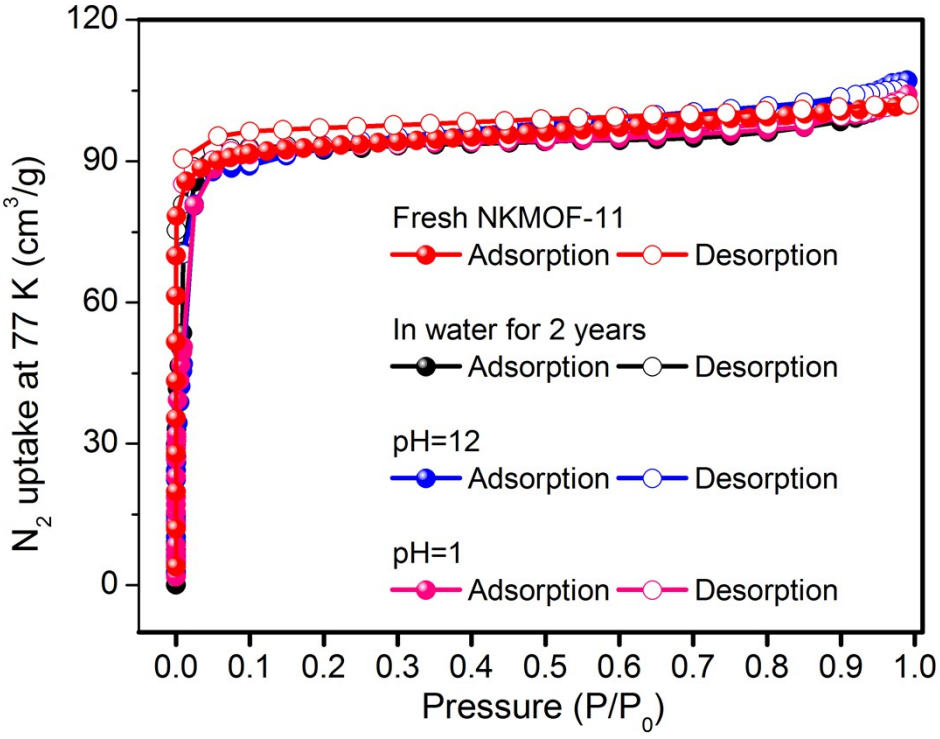

Fig. S6 The schematic of measured BET (N_2) of **NKMOF-11**. Pristine **NKMOF-11** (black); **NKMOF-11** soaked in pure water for 2 year (red); **NKMOF-11** soaked in pH=12 aqueous solution (blue); **NKMOF-11** soaked in pH=1 aqueous solution (pink).

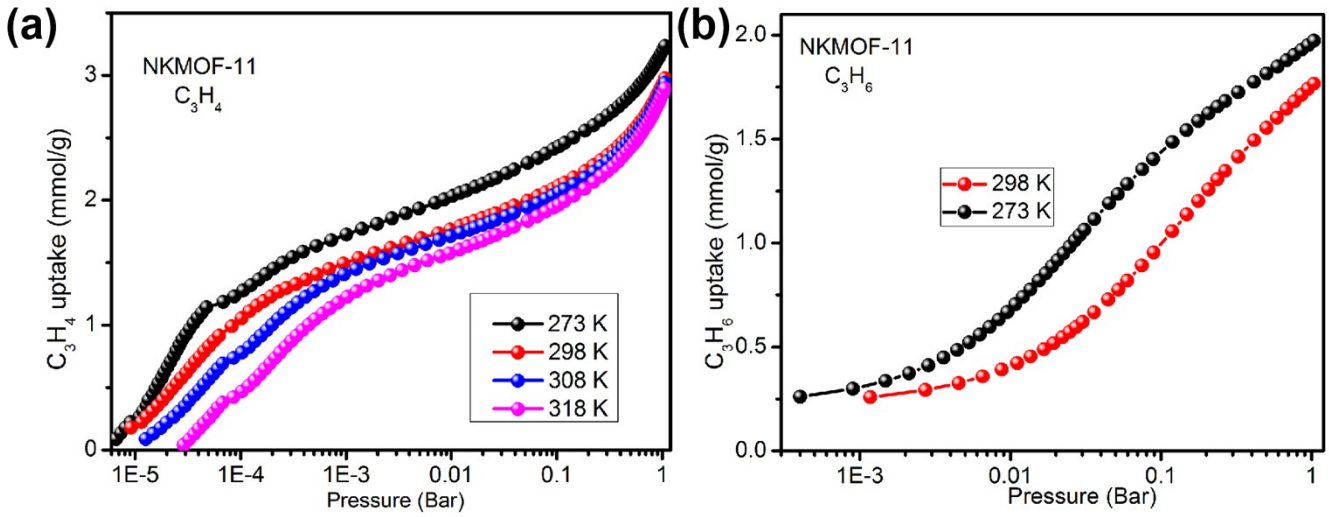

Fig. S7 The schematic of C_3H_4 and C_3H_6 single component gas adsorption isotherm for **NKMOF-11**. (a) C_3H_4 for **NKMOF-11**. (b) C_3H_6 for **NKMOF-11**.

Table S1. The fitted parameters for the DSLF equation for the C_3H_4 adsorption isotherms for **NKMOF-11** at 298, 308, and 318 K. The R^2 values are also provided.

Parameter	**298 K**	**308 K**	**318 K**
n_{m1} (mmol g^{-1})	2341.9304	3368.4332	809.9221
b_1 (kPa^{-1})	1.2345E-04	5.3343E-05	2.4600 E-04
t_1	2.9055	2.3330	2.3626
n_{m2} (mmol g^{-1})	1.4602	1.5540	1.4067
b_2 (kPa^{-1})	240.3585	61.2466	58.1809
t_2	0.9708	1.0898	0.9335
R^2	0.9983	0.9985	0.9988

Table S2. The fitted parameters for the DSLF equation for the C_3H_6 adsorption isotherms for **NKMOF-11** at 273, and 298 K. The R^2 values are also provided.

Parameter	**273 K**	**298 K**
n_{m1} (mmol g^{-1})	3.4448	1.6770
b_1 (kPa^{-1})	1.6400E-02	2.4200E-02
t_1	2.0773	1.8672
n_{m2} (mmol g^{-1})	1.3275	1.3183

b_2 (kPa^{-1})	0.4384	0.12364
t_2	1.0610	1.1266
R^2	0.9999	0.9999

Table S3. DSLF parameter fits for C_3H_6 in **NKMOF-11** as obtained through simultaneous fitting of the adsorption isotherms at 273 and 298 K.

	Site 1				Site 2				
	n_{m1}	b_{01}	E_1	t_1	n_{m2}	b_{02}	E_2	t_2	R^2
NKMOF-11	0.4080	3.62E-07	17.74683	0.6711	1.6247	3.70E-07	31.5227	1.16112	0.9999

Table S4. DSLF parameter fits for C_3H_4 in **NKMOF-11** as obtained through simultaneous fitting of the adsorption isotherms at 298 and 308 K.

	Site 1				Site 2				
	n_{m1}	b_{01}	E_1	t_1	n_{m2}	b_{02}	E_2	t_2	R^2
NKMOF-11	1.5367	3.29E-08	54.9751	1.0609	25.3496	1.65E-03	4.0528	2.4294	0.9982

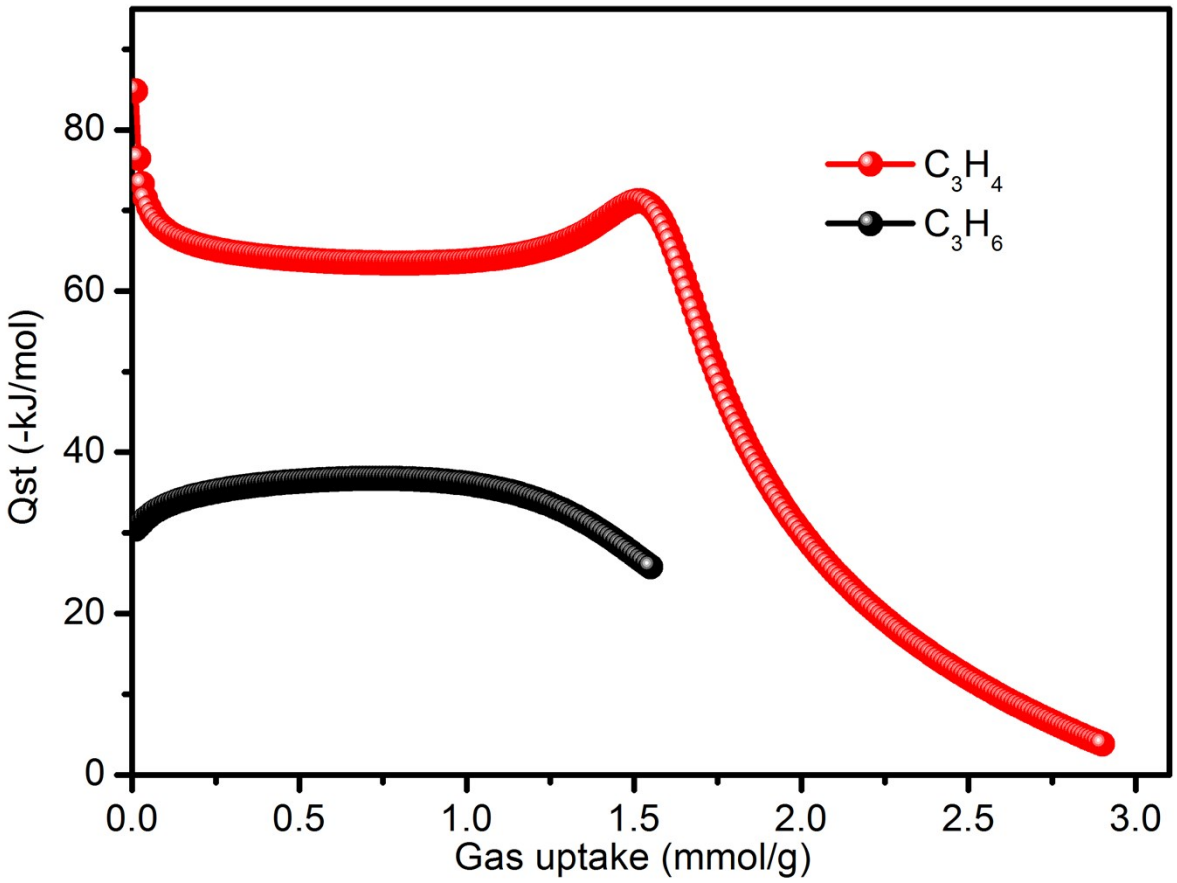

Fig. S8 Q_{st} curves of C_3H_4 and C_3H_6 for and **NKMOF-11** as obtained using Clausius-Clapeyron equation.

Table S5. Breakthrough calculations for separation of C_3H_4/C_3H_6 (1/99 and 1/999 (v/v)) mixture at 298 K.

Sorbent	Breakthrough productivity of C_3H_6 (mol/L)	
	C_3H_4/C_3H_6 (1/99, v/v)	C_3H_4/C_3H_6 (1/999, v/v)
NKMOF-11	271.7	1404.7
SIFSIX-3-Ni	185.6	285.1
SIFSIX-2-Cu-i	51.0	57.3
ELM-12[28]	94.6	110.2
ZU-62[29]	123.2	184.2

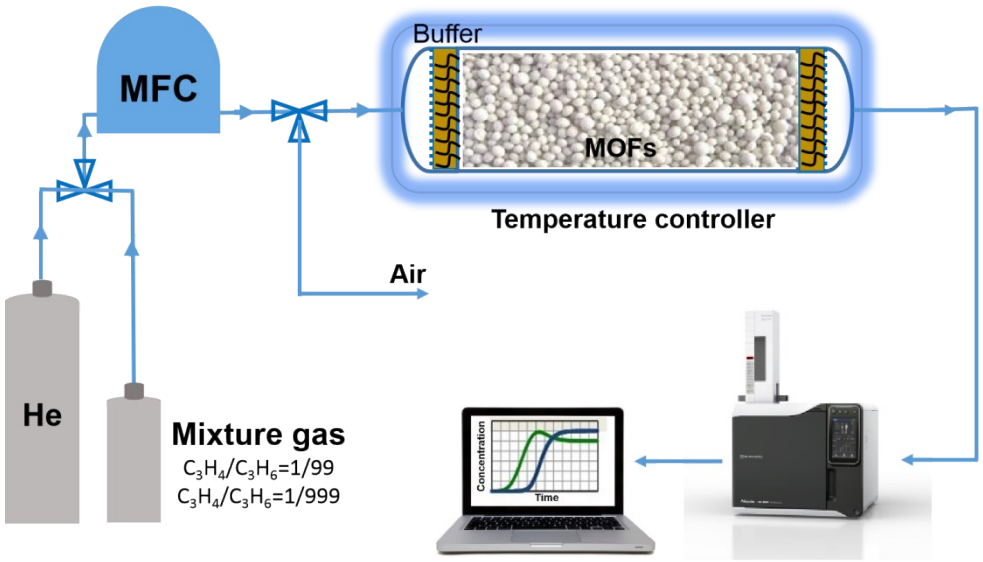

Scheme S1. Breakthrough separation apparatus.

Table S6. Comparisons of the breakthrough columns parameters studied in this work.

Sorbent	Sample weight (g)	Crystal density (g/cm^3)	Packing density (g/cm^3)	Column voidage	Column free space (cm^3)
NKMOF-11	0.102	1.713	0.850	0.504	0.060
SIFSIX-3-Ni	0.105	1.770	0.875	0.506	0.061
SIFSIX-2-Cu-i	0.103	1.423	0.858	0.397	0.048

[a] Packing density = Sample weight / Column volume (The valid column volume in this work is 0.12 cm^3).

[b] Column voidage = 1- Sample weight / Crystal density / Column volume.

[c] Column free space = Column volume × Column voidage.

Table S7. Comparisons of pure C_3H_6 (C_3H_4 < 0.1 ppm) productivities in a single breakthrough operation using C_3H_4/C_3H_6 (1/99 v/v) and (1/999 v/v) mixtures as input.

Sorbent	Crystal density (g/cm^3)	Gravimetric/Volumetric C_3H_6 Productivity (mmol/g and mmol/cm^3) of different gases mixtures	
		C_3H_4/C_3H_6 (1/99 v/v) (C_3H_4 < 1 ppm)	C_3H_4/C_3H_6 (1/999 v/v) (C_3H_4 < 1 ppm)
NKMOF-11	1.713	74.4/127.5	165.1/282.7
SIFSIX-3-Ni	1.770	--	69.5/123.0
SIFSIX-2-Cu-i	1.423	29.0/41.2	--
UTSA-200[2c]	1.417	62.05 / 87.92	142.86 / 202.43

Modeling Studies

A. Parametrization

The single X-ray crystallographic structure that was collected herein for **NKMOF-11** was used for the parametrizations and simulations in this work.

For the purpose of classical molecular simulations of propyne, and propylene adsorption in **NKMOF-11**, all atoms of the MOF were given Lennard-Jones 12–6 parameters (ε and σ),[6] point partial charges, and scalar point polarizabilities to model repulsion/dispersion, stationary electrostatic, and many-body polarization interactions, respectively. The Lennard-Jones parameters for all C and H atoms were taken from the Optimized Potentials For Liquid Simulations – All Atom (OPLS-AA) force field,[7] while such parameters for the N, S, Ni, and Cu atoms were taken from the Universal Force Field (UFF).[8]

The crystal structure of **NKMOF-11** contains 7 atoms in chemically distinct environments (**Fig. S9**). The partial charges for each unique atom were determined through electronic structure calculations on different gas phase fragments that were selected from the crystal structure of the MOF. For these calculations, all C, H, N, and S atoms were treated with the 6-31G* basis set,[9] while the LANL2DZ ECP basis set[10] was used for the Cu^{2+} and Ni^{2+} ions. The NWChem *ab initio* simulation package[11]was used to calculate the electrostatic potential surface for each fragment and the partial charges were subsequently fitted onto the atomic positions of the fragments using the CHELPG method.[12] For each chemically distinct atom, the partial charges were averaged between the fragments. The partial charges were then adjusted so that the total charge of the system was equal to zero. The resulting partial charges for each chemically distinguishable atom in **NKMOF-11** are provided in **Table S8**. The exponential damping-type polarizability values for all C, H, N, and S atoms were taken from a carefully parametrized set provided by the work of van Duijnen and Swart.[13] The polarizability parameter for Ni^{2+} and Cu^{2+} were determined in previous work[14]and used for the simulations herein.

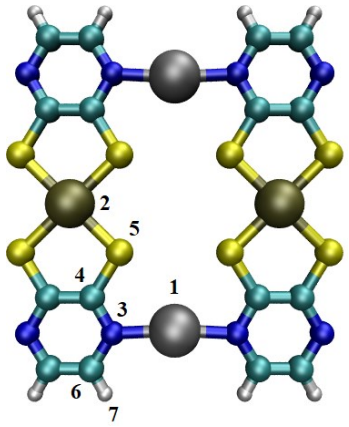

Fig. S9. The numbering of the chemically distinct atoms in **NKMOF-11** as referred to in **Table S8**. Atom colors: C = cyan, H = white, N = blue, S = yellow, Ni = silver, Cu = gold.

Table S8: The partial charges (in e^-) for the chemically distinct atoms in **NKMOF-11** that were used for the GCMC simulations in this work. Label of atoms correspond to **Figure S8**.

Atom	Label	*q* (e^-)
Ni	1	1.3031
Cu	2	0.5737
N	3	–0.5272
C	4	0.2001
S	5	–0.2983
C	6	0.0380
H	7	0.1182

B. Grand Canonical Monte Carlo

Molecular simulations of propyne and propene adsorption were performed in **NKMOF-11** using grand canonical Monte Carlo (GCMC) methods [15] within a 3 × 3 × 2 supercell of the MOF. A spherical cut-off distance of 10.2396 Å was used for the simulations; this value corresponds to half the shortest supercell dimension length. Propyne, and propylene were modeled using recently developed polarizable potentials of the respective adsorbates.[16] The total potential energy of the MOF-adsorbate system was calculated through the sum of the repulsion/dispersion, stationary electrostatic, and polarization energies. These were calculated using the Lennard-Jones 12-6 potential, partial charges with Ewald summation,[17] and a Thole-Applequist type model,[18] respectively. All MOF atoms were kept fixed throughout the simulations. All GCMC simulations were performed using the Massively Parallel Monte Carlo (MPMC) code.[19]

According to the simulations, saturation of propyne and propene in **NKMOF-11** is achieved at 2.5 and 2 molecules per unit cell, respectively. The modeled 3 × 3 × 2 supercell of the MOF containing the saturated loading amount for propyne and propene are shown in **Fig. S10** and **S11**, respectively. Consistent with previous experimental and theoretical findings for these adsorbates in the isostructural **NKMOF-1-Cu** and **NKMOF-1-Ni**, all C3 hydrocarbons adsorbed at two main binding sites in **NKMOF-11**: (1) between the pyrazine units and (2) between the CuS_4 units.

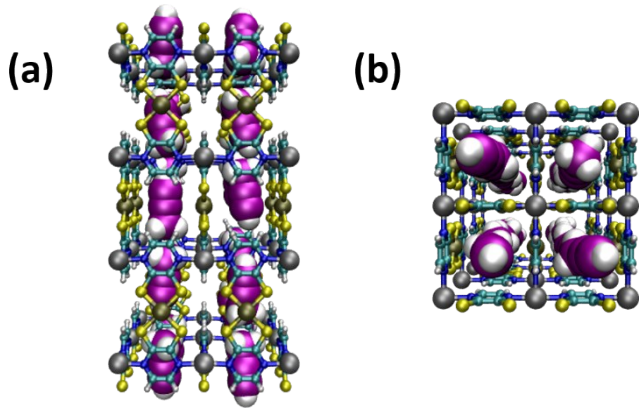

Fig. S10 (a) Perspective *a/b*-axis view and (b) *c*-axis view of the modeled 3 × 3 × 2 supercell in **NKMOF-11** at propyne saturation. Atom colors: C(MOF) = cyan, C(propyne) = magenta, H = white, N = blue, S = yellow, Ni = silver, Cu = gold.

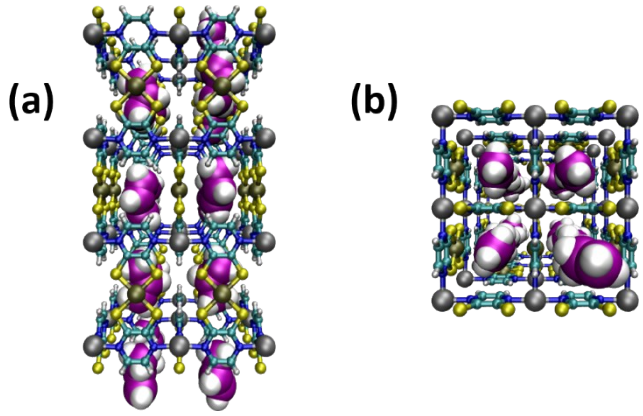

Fig. S11 (a) Perspective *a/b*-axis view and (b) *c*-axis view of the modeled 3 × 3 × 2 supercell in **NKMOF-11** at propene saturation. Atom colors: C(MOF) = cyan, C(propene) = magenta, H = white, N = blue, S = yellow, Ni = silver, Cu = gold.

C. Density Functional Theory

Periodic density functional theory (DFT) calculations were performed to evaluate the adsorption energy (ΔE) for propyne, and propylene about the two adsorption sites in **NKMOF-11**. These calculations were performed using the Vienna *ab initio* Simulation Package (VASP)[20] with the projector augmented wave (PAW) method,[21] Perdew-Burke-Ernzerhof (PBE) functional,[22] and the DFT-D2 correction method of Grimme.[23] For both sites, the position of a single molecule of each adsorbate was initially optimized within the rigid unit cell of the MOF. Afterward, another optimization was carried out in which the position of all atoms and lattice parameters of the system were allowed to vary. All optimizations were converged to within 10^{-6} eV. The optimized position of a propyne, and propylene molecule about both sites within **NKMOF-11** are displayed in **Fig. 5,** and **Fig. S12**, respectively.

The ΔE for the adsorbates localized about the two binding sites in **NKMOF-11** were calculated by the following:
$\Delta E = E(\text{MOF + Adsorbate}) - E(\text{MOF}) - E(\text{Adsorbate})$
where E(MOF + Adsorbate) is the energy of the unit cell of the MOF with the adsorbate, E(MOF) is the energy of the empty unit cell, and E(Adsorbate) is the energy of the adsorbate. The calculated ΔE values for propyne, and propene about both sites in **NKMOF-11** are listed in **Table S9**.

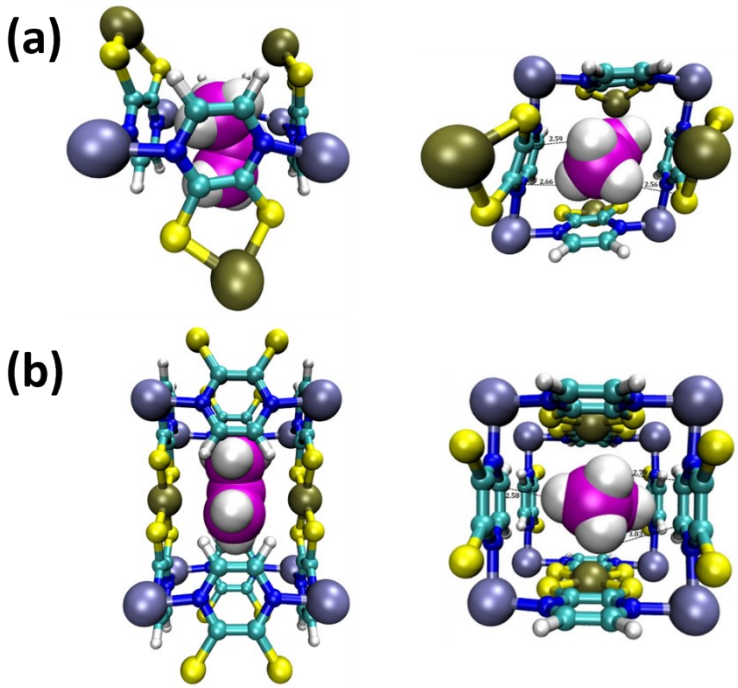

Fig. S12 Perspective views (left = *a*/*b*-axis, right = *c*-axis) of a portion of the crystal structure of **NKMOF-11** showing the optimized position of a propylene molecule about (a) the pyrazine units and (b) the CuS_4 units in the MOF as determined through periodic DFT calculations using VASP. The closest MOF-adsorbate distances are also shown. Atom colors: C(MOF) = cyan, C(propylene) = magenta, H = white, N = blue, S = yellow, Ni = silver, Cu = gold.

Table S9. Calculated adsorption energies (in kJ mol^{-1}) for a single propyne, and propylene molecule at two sites in **NKMOF-11** as determined from periodic DFT calculations using VASP. Site 1 corresponds to adsorption between the pyrazine units and site 2 is between the CuS_4 units.

Adsorbate	**Site**	**Δ*E* (kJ mol^{-1})**
Propyne	1	–70.09
	2	–54.11
Propylene	1	–43.32
	2	–55.68

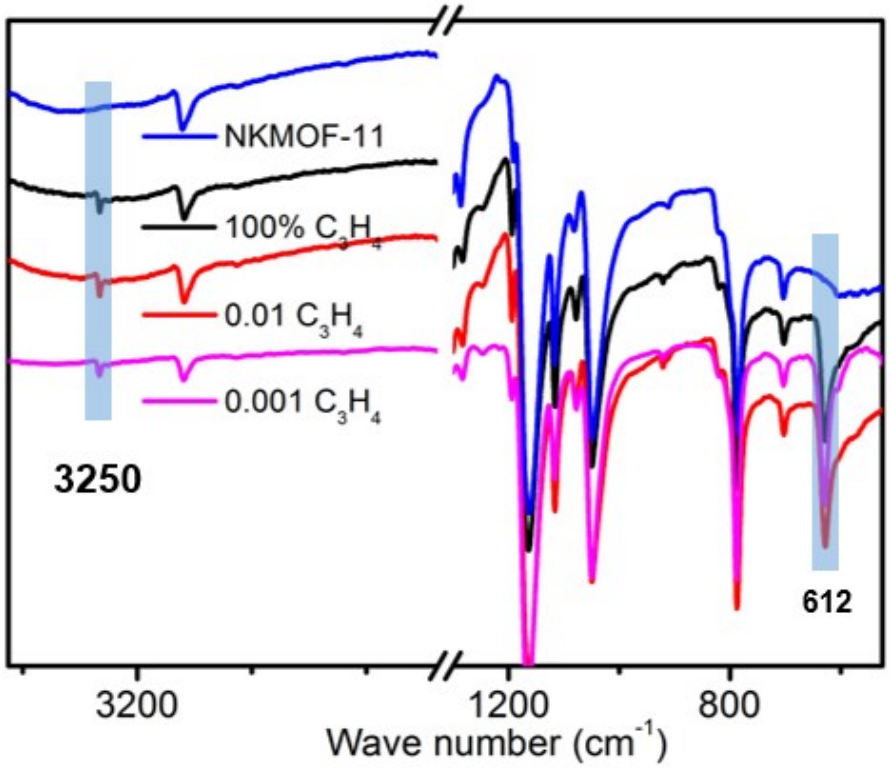

Fig. S13 The schematic of FT-IR of **NKMOF-11** absorbed C_3H_4 from gas mixture containing C_3H_4. Two characteristic peaks of C_3H_4 were highlighted in blue.

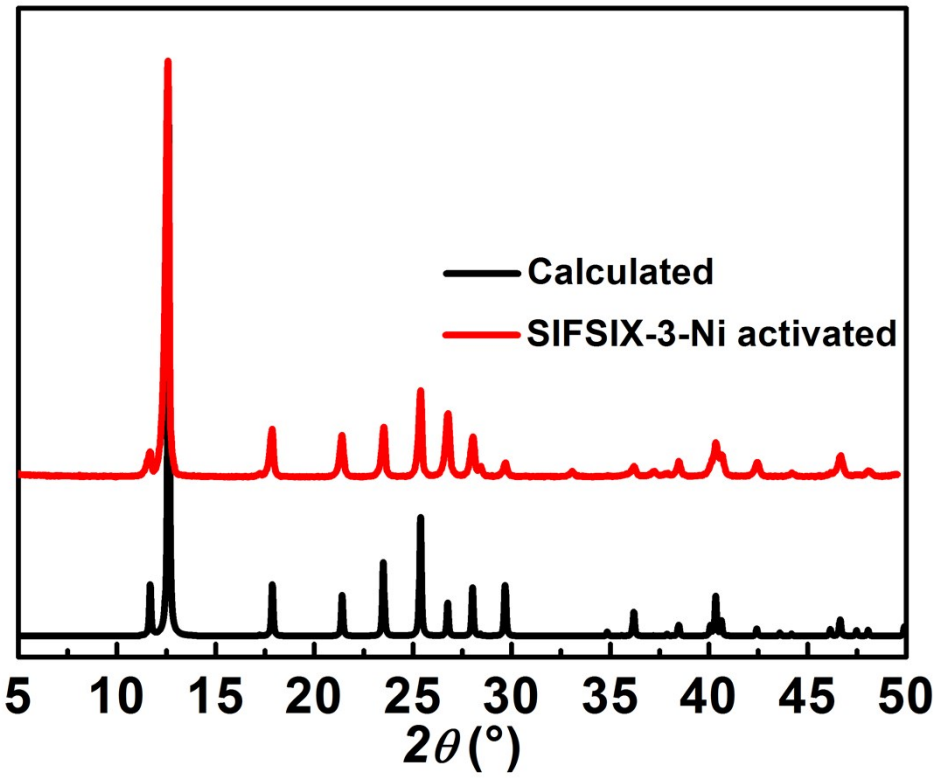

Fig. S14 PXRD patterns of the calculated and activated **SIFSIX-3-Ni**.

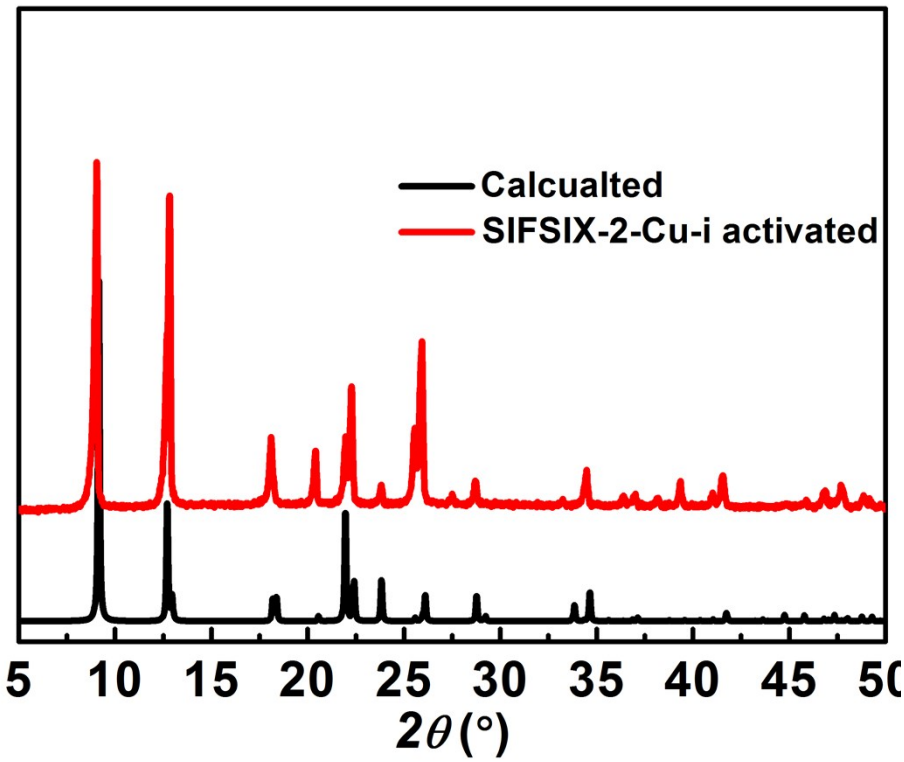

Fig. S15 PXRD patterns of the calculated, activated **SIFSIX-2-Cu-i**.

Simulated transient breakthrough of mixtures in fixed bed adsorbers

The performance of industrial fixed bed adsorbers is dictated by a combination of adsorption selectivity and uptake capacity. Transient breakthrough simulations were carried out for 1/99 $C_3H_4(1)/C_3H_6$ and 1/999 $C_3H_4(1)/C_3H_6$ mixtures operating at a total pressure of 100 kPa and 298 K, using the methodology described in earlier publications.[24-27] For the breakthrough simulations, the following parameter values were used: length of packed bed, *L* = 0.3 m; voidage of packed bed, ε = 0.4; superficial gas velocity at inlet, μ = 0.04 m/s.

The transient breakthrough simulation results are presented in terms of a *dimensionless* time, τ, defined by dividing the actual time, *t*, by the characteristic time, $L\varepsilon/u$.

For comparisons of the separation performance, we plot the ppm C_3H_4 in the gaseous product mixture leaving the adsorber as a function of the dimensionless time, τ. The breakthrough data are provided in Figure 3.

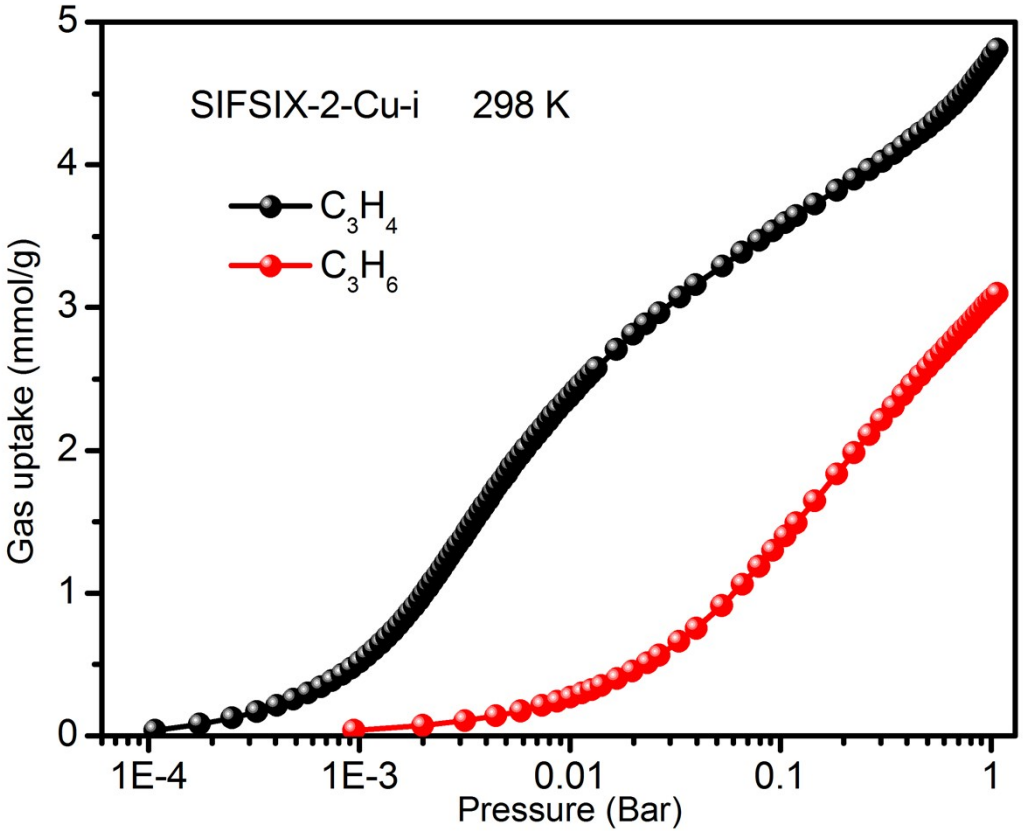

Fig. S16 The schematic of C_3H_4 and C_3H_6 gas adsorption isotherms for **SIFSIX-2-Cu-i** at 298 K.

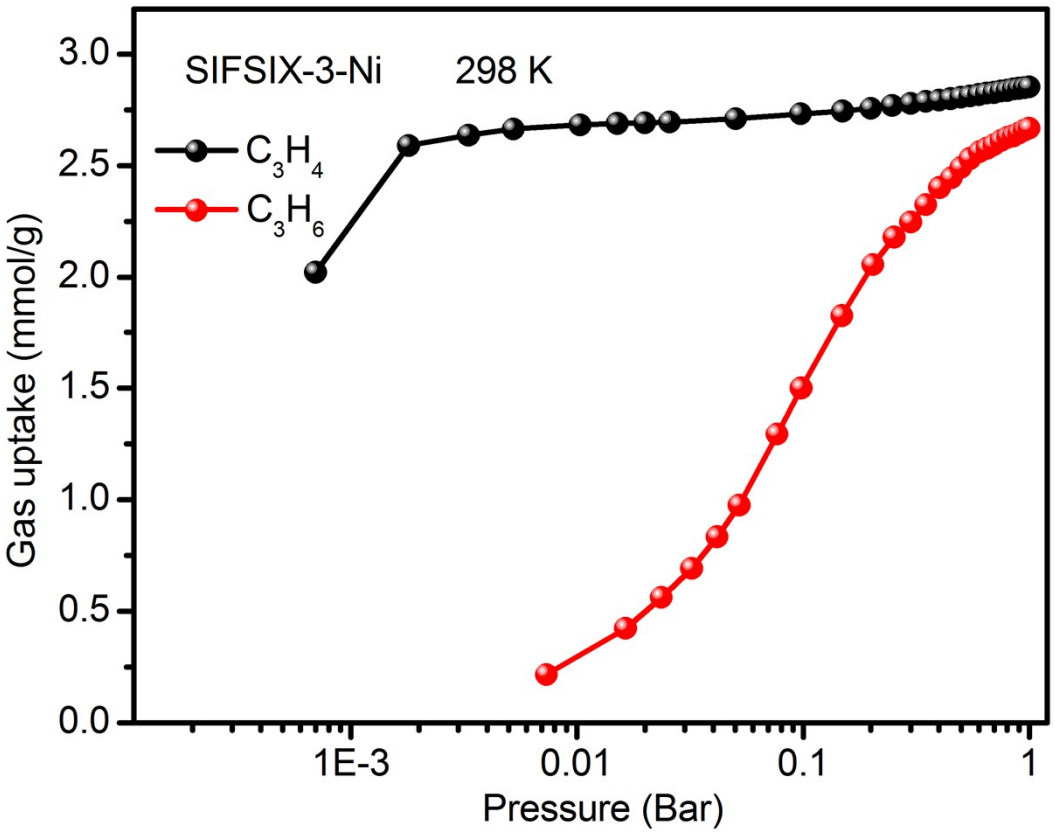

Fig. S17 The schematic of C_3H_4 and C_3H_6 gas adsorption isotherm for **SIFSIX-3-Ni** at 298 K.

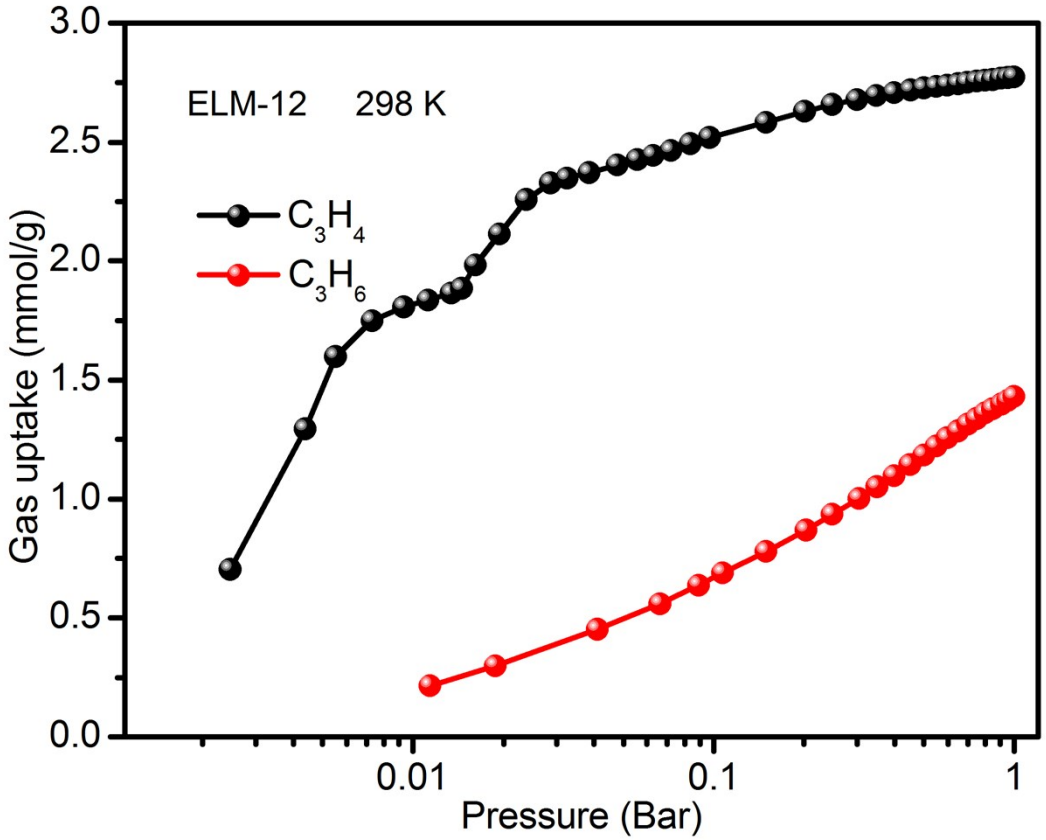

Fig. S18 The schematic of C_3H_4 and C_3H_6 gas adsorption isotherm for **ELM-12** at 298 K.

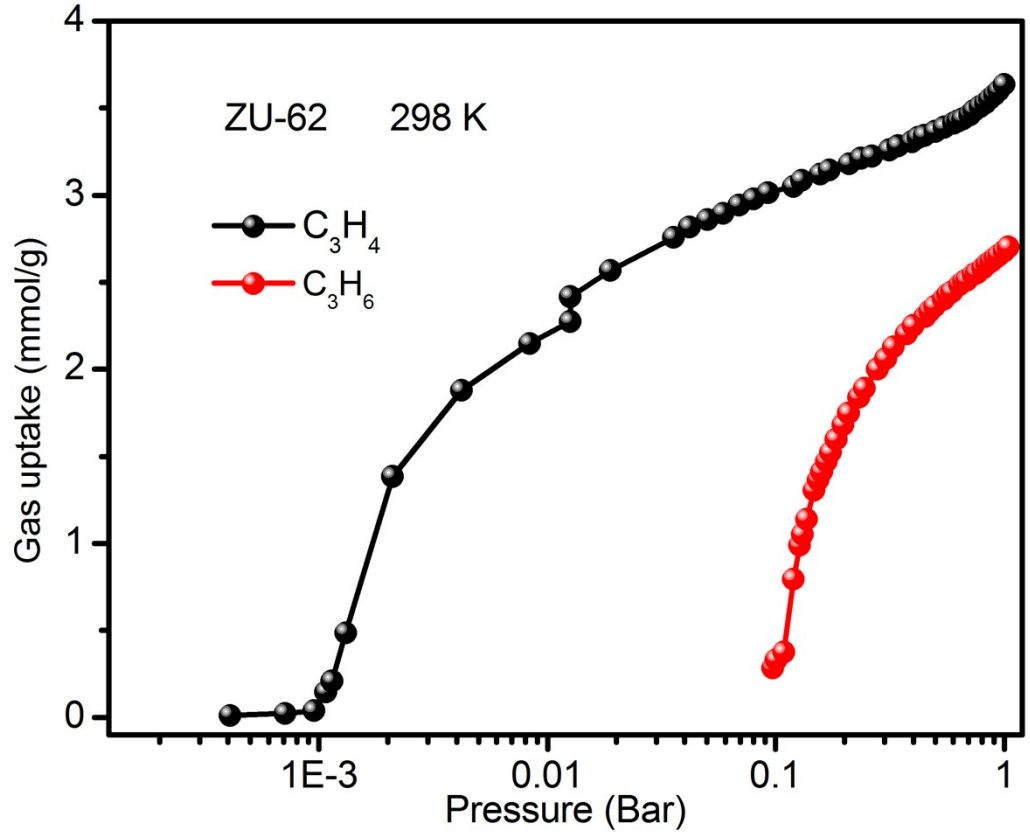

Fig. S19 The schematic of C_3H_4 and C_3H_6 gas adsorption isotherm for **ZU-62** at 298 K.

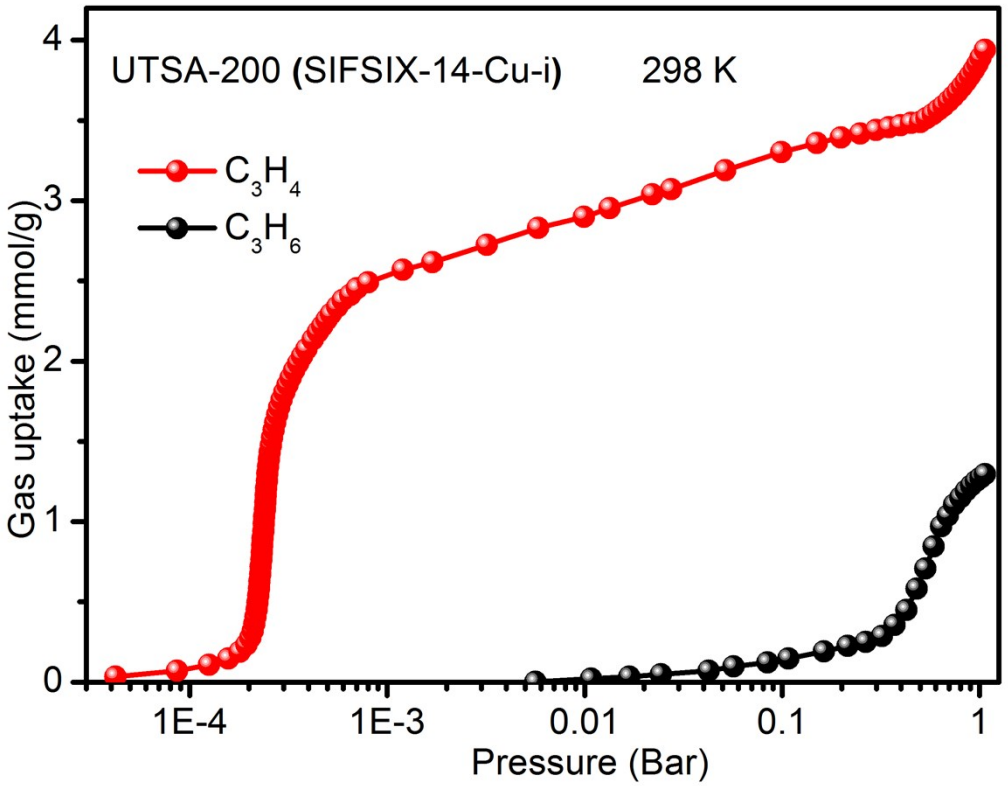

Fig. S20 The schematic of C_3H_4 and C_3H_6 gas adsorption isotherm for **UTSA-200 (SIFSIX-14-Cu-i)** at 298 K.

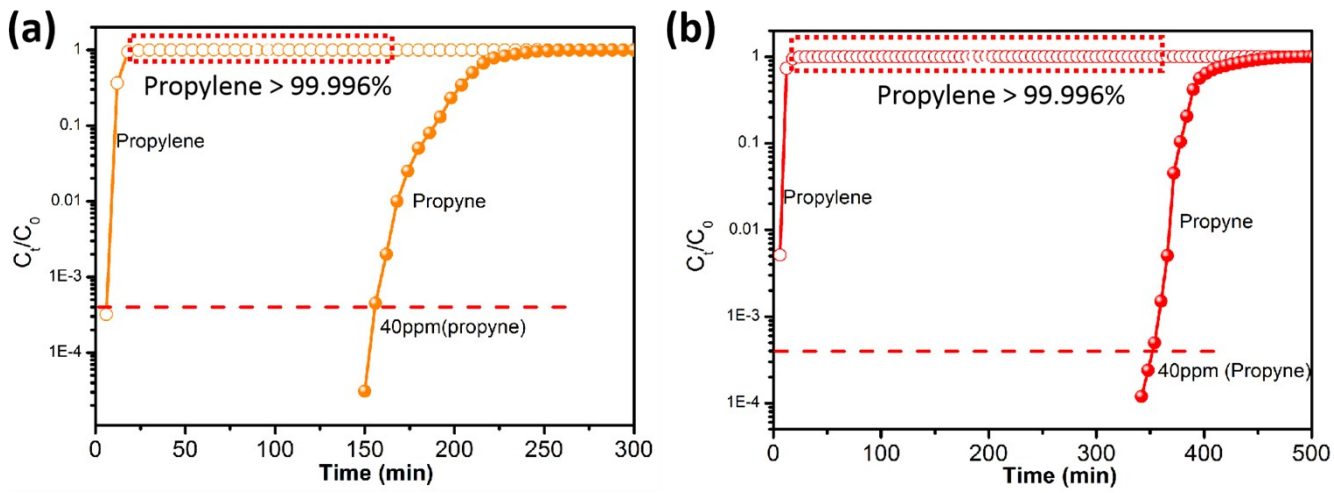

Fig. S21 (a) The concentrations of propylene in breakthrough experiments of **NKMOF-11** for propyne/propylene (1/99, v/v) and (b) for propyne/propylene (1/999, v/v).

Notation

b	Langmuir-Freundlich constant, $\mathrm{Pa}^{-\nu}$
q	component molar loading of species i, mol kg^{-1}
q_{sat}	saturation loading, mol kg^{-1}
L	length of packed bed adsorber, m
t	time, s
T	absolute temperature, K
u	superficial gas velocity in packed bed, m s^{-1}

Greek letters

ε	voidage of packed bed, dimensionless
ν	Freundlich exponent, dimensionless
ρ	crystal framework density, kg L^{-1}
τ	time, dimensionless

References

1 Y.-L. Peng, T. Pham, P. Li, T. Wang, Y. Chen, K.-J. Chen, K. A. Forrest, B. Space, P. Cheng, M. J. Zaworotko, Z. Zhang, *Angew. Chem. Int. Ed.* 2018, **57**, 10971-10975.

2 a) K.-J. Chen, Hayley S. Scott, David G. Madden, T. Pham, A. Kumar, A. Bajpai, M. Lusi, Katherine A. Forrest, B. Space, John J. Perry, Michael J. Zaworotko, *Chem* 2016, **1**, 753-765. b) x. Cui, K-J Chen, H. Xing, Q. Yang, R. Krishna, Z. Bao, H. Wu, W. Zhou, X. Dong, Y. Han, B Li, Q. Ren, M. J. Zaworotko, B. Chen, *Science* 2016, **353**, 141-144; c) L. Li, H.-M. Wen, C. He, R.-B. Lin, R. Krishna, H. Wu, W. Zhou, Ji. Li, B. Li, B. Chen, *Angew. Chem. Int. Ed.* 2018, **130**, 17.

3 R. T. Yang, *Gas separation by adsorption processes*, Butterworth-Heinemann, 1986.

4 H. Pan, J. A. Ritter, P. B. Balbuena, *Langmuir* 1998, **14**, 6323-6327.

5 U. W. F. S, *Journal of the Institute of Actuaries* 1924, **55**, 202-203.

6 J. E. Jones, S. Chapman, *Proceedings of the Royal Society of London. Series A, Containing Papers of a Mathematical and Physical Character* 1924, **106**, 463-477.

7 W. L. Jorgensen, D. S. Maxwell, J. Tirado-Rives, *J. Am. Chem. Soc.* 1996, **118**, 11225-11236.

8 A. K. Rappe, C. J. Casewit, K. S. Colwell, W. A. Goddard, W. M. Skiff, *J. Am. Chem. Soc.* 1992, **114**, 10024-10035.

9 a) P. C. Hariharan, J. A. Pople, *Theoretica chimica acta* 1973, **28**, 213-222; b) M. M. Francl, W. J. Pietro, W. J. Hehre, J. S. Binkley, M. S. Gordon, D. J. DeFrees, J. A. Pople, *The Journal of Chemical Physics* 1982, **77**, 3654-3665.

10 a) W. J. Stevens, H. Basch, M. Krauss, *The Journal of Chemical Physics* 1984, **81**, 6026-6033; b) P. J. Hay, W. R. Wadt, *The Journal of Chemical Physics* 1985, **82**, 270-283; c) L. A. LaJohn, P. A. Christiansen, R. B. Ross, T. Atashroo, W. C. Ermler, *The Journal of Chemical Physics* 1987, **87**, 2812-2824.

11 M. Valiev, E. J. Bylaska, N. Govind, K. Kowalski, T. P. Straatsma, H. J. J. Van Dam, D. Wang, J. Nieplocha, E. Apra, T. L. Windus, W. A. de Jong, *Comput. Phys. Commun.* 2010, **181**, 1477-1489.

12 (a) L. E. Chirlian, M. M. Francl, *J. Comput. Chem.* 1987, **8**, 894-905; (b) C. M. Breneman, K. B. Wiberg, *J. Comput. Chem.* 1990, **11**, 361-373.

13 P. T. van Duijnen, M. Swart, *The Journal of Physical Chemistry A* 1998, **102**, 2399-2407.

14 a) T. Pham, K. A. Forrest, R. Banerjee, G. Orcajo, J. Eckert, B. Space, *The Journal of Physical Chemistry C* 2015, **119**, 1078-1090; b) K. A. Forrest, T. Pham, K. McLaughlin, J. L. Belof, A. C. Stern, M. J. Zaworotko, B. Space, *The Journal of Physical Chemistry C* 2012, **116**, 15538-15549.

15 N. Metropolis, A. W. Rosenbluth, M. N. Rosenbluth, A. H. Teller, E. Teller, *The Journal of Chemical Physics* 1953, **21**, 1087-1092.

16 Y.-L. Peng, C. He, T. Pham, T. Wang, P. Li, R. Krishna, K. A. Forrest, A. Hogan, S. Suepaul, B. Space, M. Fang, Y. Chen, M. J. Zaworotko, J. Li, L. Li, Z. Zhang, P. Cheng, B. Chen, *Angew. Chem. Int. Ed.* 2019, **58**, 10209-10214.

17 B. A. Wells, A. L. Chaffee, *Journal of Chemical Theory and Computation* 2015, **11**, 3684-3695.

18 a) J. Applequist, J. R. Carl, K.-K. Fung, *J. Am. Chem. Soc.* 1972, **94**, 2952-2960; b) B. T. Thole, *Chem. Phys.* 1981, **59**, 341-350; c) K. A. Bode, J. Applequist, *The Journal of Physical Chemistry* 1996, **100**, 17820-17824; (d) K. McLaughlin, C. R. Cioce, T. Pham, J. L. Belof, B. Space, *The Journal of Chemical Physics* 2013, **139**, 184112.

[9 a) D. M. Franz, J. L. Belof, K. McLaughlin, C. R. Cioce, B. Tudor, A. Hogan, L. Laratelli, M. Mulcair, M. Mostrom, A. Navas, A. C. Stern, K. A. Forrest, T. Pham, B. Space, *Advanced Theory and Simulations* 2019, **2**, 1900113.

20 a) G. Kresse, J. Hafner, *Physical Review B* **1993**, *47*, 558-561; b) G. Kresse, J. Hafner, *Physical Review B* **1994**, *49*, 14251-14269; c) G. Kresse, J. Furthmüller, *Physical Review B* 1996, **54**, 11169-11186.

21 a) P. E. Blöchl, *Physical Review B* **1994**, *50*, 17953-17979; b) G. Kresse, D. Joubert, *Physical Review B* 1999, **59**, 1758-1775.

22 J. P. Perdew, K. Burke, M. Ernzerhof, *Phys. Rev. Lett.* 1996, **77**, 3865-3868.

23 S. Grimme, *J. Comput. Chem.* 2006, **27**, 1787-1799.

24 R. Krishna, *RSC Advances* 2017, **7**, 35724-35737.

25 R. Krishna, *Microporous Mesoporous Mater.* 2014, **185**, 30-50.

26 R. Krishna, *RSC Advances* 2015, **5**, 52269-52295.[27] R. Krishna, *Sep. Purif. Technol.* 2018, **194**, 281-300.